Migration technique based on the time-domain model of the Ground Penetrating Radar

Bart Scheers[*a], Marc Acheroy[*a], André Vander Vorst[*b]
[a]ELTE Dep., Royal Military Academy,1000 Brussels., Belgium
[b]Hyperfréquences U.C.L., Belgium

ABSTRACT

Migration is a common name for processing techniques that try to reconstruct, from the data recorded at the surface, the reflecting structures in the sub-surface. Most of the existing migration techniques do not take into account the characteristics of the acquisition system and the ground characteristics. We propose a novel migration method, applicable on Ground Penetrating Radar (GPR) images, that integrates the time domain model of the GPR in the migration scheme. We calculate by forward modelling a synthetic 3D point spread function of the GPR, *i.e.* a synthetic C-scan of a small point scatterer. The 3D point spread function, containing system characteristics like the waveform of the excitation source, the combined antenna footprint and the impulse response (IR) of the antennas, is then used to deconvolve the recorded data. Results of this migration method on real data obtained by an ultra-wideband GPR system show that the migration method is able to reconstruct the top contour of small targets like AP mines, in some cases even with the correct dimensions. The method is also capable of migrating oblique targets into their true position. The migration scheme is not computational intensive and can easily be implemented in real time.

Keywords: Humanitarian demining, UWB GPR, time domain modelling, migration.

1. INTRODUCTION

In images taken by a GPR, the reflections on structures in the sub-surface will be smeared out over a broad region and will appear as hyperbolic structures in the image. This is due to the beam-width of transmit and receive antenna. The aim of migration techniques is to focus target reflections in the recorded data back into their true position and physical shape. In this respect, migration can be seen as a form of spatial deconvolution that increases spatial resolution. The first migration methods were geometric approaches. After the introduction of the computer, more complex techniques, based on the scalar wave equation, were introduced. These methods involve back-propagation or inverse extrapolation to remove the effects of wave field propagation. A good overview of migration techniques is given in [1] [2]. Most of the migrations methods found their origin in the field of seismic, and were later on also applied on radar images. Almost none of these methods however include system aspects of the radar like the waveform of the excitation source, the impulse response of the antennas, the antenna pattern, *etc.* Furthermore most of the migration methods consider the ground as being loss-less and without dispersion. It can be expected that a migration technique that takes into account the characteristics of the radar system and possibly the characteristics of the ground would perform better. In this paper we present a novel migration method that takes into account the system and ground characteristics.

2. TIME-DOMAIN MODEL OF THE GPR

A key element in the migration method is the point-spread function of the GPR, *i.e.* a synthetic C-scan of a small point scatterer. This point spread function can be obtained by forward modelling, using a time-domain model of the GPR system. The time-domain model is obtained by considering the total system " GPR-ground-target" as a cascade of linear responses, resulting in a *time-domain GPR range equation*. The time-domain GPR range equation allows us to calculate the received voltage $V_{rec}(t)$ at the output of the receiving antenna in terms of excitation voltage $V_S(t)$, radar characteristics and target. Fig. 1 shows a schematic representation of the different parts in this cascade, *e.g.* the pulse generator, the antennas modelled by their normalised impulse response [3][4], the 1/R spreading losses, the transmission coefficients on the air-ground interface, the propagation through the ground and the scattering on the target in the ground.

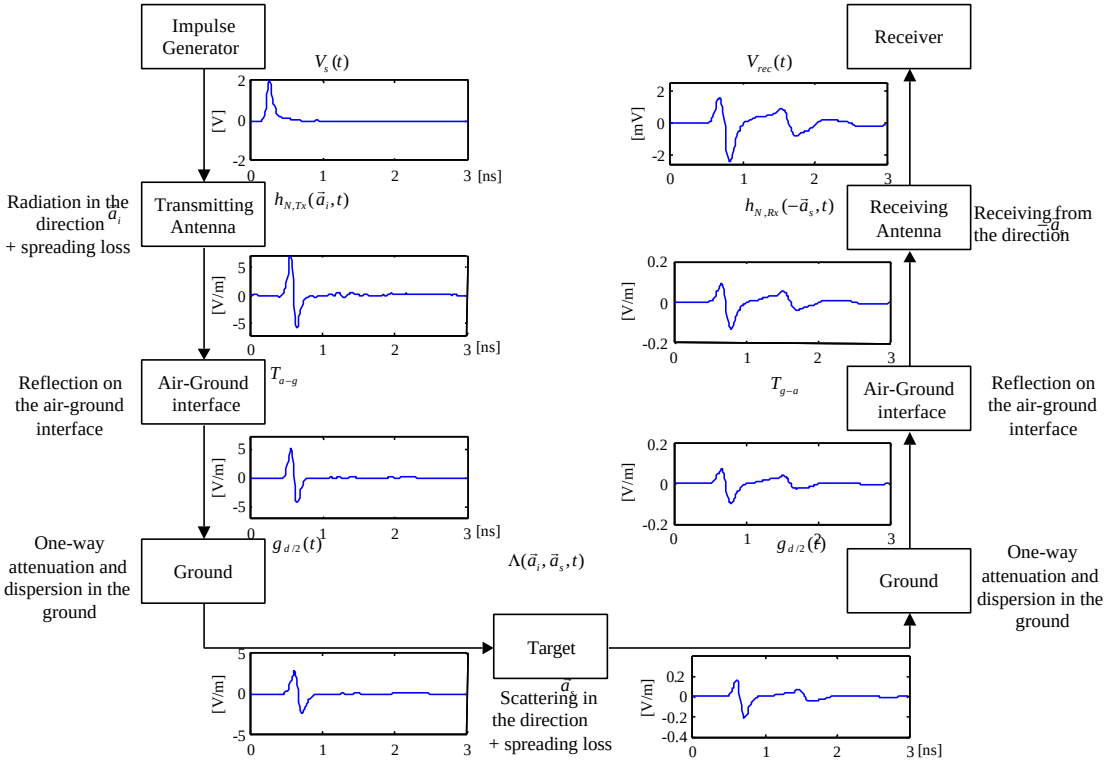

Fig. 1: Schematic representation of the different parts in the time-domain GPR range equation

Mathematically the time domain GPR range equation is expressed as

$$V_{rec}(t) = \frac{T_{a-g}.T_{g-a}}{8p^2 R_t R_r c} g_d(t) \otimes h_{N,Tx}(\vec{a}_i,t) \otimes \Lambda_{1,1}(\vec{a}_i,\vec{a}_s,t) \otimes h_{N,Rx}(-\vec{a}_s,t) \otimes \frac{dVs(t)}{dt} \qquad \textbf{(1)}$$

with

$V_S(t)$: the excitation voltage applied at the transmitting antenna

$h_{N,Tx}(\vec{a}_i,t)$: the normalised IR of the transmitting antenna in the direction $\vec{a}_i$

$h_{N,Rx}(-\vec{a}_s,t)$: the normalised IR of the transmitting antenna in the direction $-\vec{a}_s$

$g_d(t)$: the impulse response representing the two-way path length loss and the dispersion in the ground

$\Lambda_{1,1}(\vec{a}_i,\vec{a}_s,t)$: the IR of the target (is the time equivalent of the square root of the target radar cross section)

R_t : the total path length from transmitting antenna to the target

R_r : the total path length from receiving antenna to the target

T_{a-g} : the transmission coefficient at the air-ground interface (air to ground)

T_{g-a} : the transmission coefficient at the air-ground interface (ground to air).

$\vec{a}_i$: the direction of radiation of the transmitting antenna towards the target

$\vec{a}_s$: the direction of the scattered field from the target towards the receiving antenna.

In the next two subsections the impulse responses of the antennas and the ground will be explained in more detail

2.1 Normalised impulse response of the antennas

A common way of describing antennas in the time domain is by means of their impulse response. Different types of IRs can be defined. We opted for the normalised impulse response (normalised IR), *i.e.* an impulse response integrating all frequency dependent antenna characteristics [3] [4]. In this way, the time domain antenna equations, expressed in terms of the normalised IR, become very simple and accurate to use. No assumptions about frequency dependent terms has to be made. For two identical antennas, $h_{N,Tx} = h_{N,Rx}$. The normalised IR on boresight is easy to measure, using two identical antennas and a vector network analyser [3]. Fig. 2 shows the normalised IR on boresight of a TEM horn antenna, designed for a laboratory UWB GPR [5].

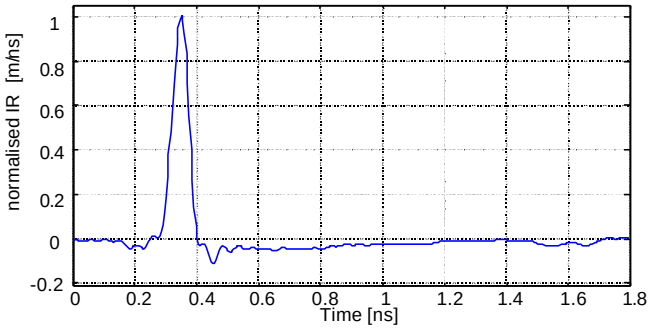

Fig. 2: Normalised IR of TEM horn antenna

2.2 Impulse response of the ground

The best way to introduce the propagation losses in the ground is to representing the ground as a low-pass filter. The transfer function of this filter, representing a propagation of *d* meters in the ground, is given by $H_d(w) = e^{-(a+jb)d}$, where α is the attenuation constant [Np/m] of the medium and β the phase constant [rad/m]. Both constants are a function of frequency, the real part of the permittivity e' and the loss tangent $\tan d$. For a given soil, i.e. texture, density and moister content, and for a given two-way path length d in the ground, the impulse response $g_d(t)$ of the soil, representing the propagation losses, is then calculated as [5]

$$g_d(t) = \frac{d\sqrt{me'}(\tan d)/2}{p\left[\left(t - d\sqrt{me'}\right)^2 + \left(d\sqrt{me'}\tan d/2\right)^2\right]} \qquad \textbf{(2)}$$

3. DEVELOPMENT OF THE MIGRATION METHOD

The migration method is based on the deconvolution of the recorded data with the point-spread function of the system, calculated using the time-domain model as presented in previous section. This deconvolution has only sense if the acquisition process by the UWB GPR is a convolution between the structures present in the subsurface and the point-spread function of the system. The latter is true under certain assumptions. Suppose a co-ordinate system as represented in Fig. 3. The antenna configuration is a bistatic configuration and there are only variations in propagation velocity in the downward direction. The 3D data $b(x, y, z = 0, t)$ are recorded on a regular grid by moving the antennas in the xy-plane at z =0.

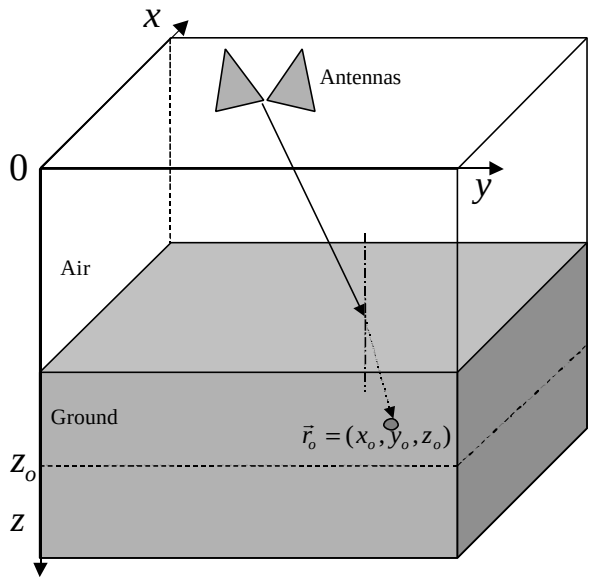

Fig. 3: Configuration and representation of the co-ordinate system

Assume in a first time that there is only one small isotropic point scatterer present in the subsurface, located at $\vec{r}_o = (x_o, y_o, z_o)$ and characterised by an impulse response $\Lambda_o(t_o)$, independent of the incident direction. Note that, in the most general case, the IR of the localised isotropic point scatterer does not necessarily have to be a Dirac impulse as a function of time. For the antennas at any position $\vec{r}_a = (x_a, y_a, z = 0)$, the received voltage, representing an A-scan, can be written according to (1) as

$$b(\vec{r}_a, t) = \frac{T_{a-g} T_{g-a}}{8p^2 R_t R_r c} g_d(t) \otimes h_{N,Tx}(\vec{a}_i, t) \otimes \Lambda_o(t) \otimes h_{N,Rx}(-\vec{a}_s, t) \otimes \frac{dVs(t - t_d)}{dt} \quad \textbf{(3)}$$

where t_d represents the exact two-way travelling time between the antennas and the point target, taking into account the different propagation velocities in the media.

By grouping all the factors, except for the IR of the point target, in one factor $w(\vec{r}_a, \vec{r}_o, t)$, equation (3) becomes

$$b(\vec{r}_a, t) = w(\vec{r}_a, \vec{r}_o, t) \otimes_t \Lambda_o(t) \quad \textbf{(4)}$$

The symbol $\otimes_t$ is introduced to clearly indicate that the convolution in (4) is a convolution in time. For a given configuration, all the factors in (3) are known, hence $w(\vec{r}_a, \vec{r}_o, t)$ can be easily calculated. Furthermore, for the antennas at $z = 0$ and the point scatterer at a fixed depth $z = z_o$, the response $w(\vec{r}_a, \vec{r}_o, t)$ is a function of $\vec{r}_o$ and $\vec{r}_a$ only by their difference, and (4) can be written as

$$b(\vec{r}_a, t) = w(\vec{r}_a - \vec{r}_o, t) \otimes_t \Lambda(r_0, t) \quad \textbf{(5)}$$

If an object can be modelled by a set of independent small isotropic point scatterers, all at approximately the same depth $z = z_o$, the output voltage $b(\vec{r}_a, t)$ will be a combination of the contribution of each individual point scatterer, that is clearly a convolution in space if we assume that the operation is linear:

$$b(x_a, y_a, t) = \iint_{x,y} \int_t w(x_a - x, y_a - y, z_o, t - t')\Lambda_{zo}(x, y, t')dt'\,dxdy \qquad \textbf{(6)}$$

Equation (6) represents a space-time convolution along the co-ordinates x, y and t, and can be written as

$$b(x, y, t) = w(x, y, z_o, t) \otimes_{x,y,t} \Lambda_{zo}(x, y, t) \qquad \textbf{(7)}$$

where $\Lambda_{zo}(x, y, t)$ is a 3D matrix, called the scattering matrix [2], and contains the responses associated with the distributed point scatterers at approximately a depth z_o. The symbol $\otimes_{x,y,t}$ denotes a space-time convolution along the co-ordinates x, y and t. The 3D matrix $w(x, y, z_o, t)$ represents the point spread function of the UWB GPR system for a depth z_o. In practice $w(x, y, z_o, t)$ is calculated by using (3) for different antenna positions $\vec{r}_a$ on a regular grid in the xy-plane at z = 0 and a small fictive point scatterer with IR $d(t)$, at a depth z_o. In other words it can be seen as a synthetic C-scan of a small fictive point scatterer. Fig. 4 shows the 3D point spread function of the system at a depth of 6 cm below the air-ground interface (with the antennas 25 cm above the ground). In the point spread function, as it is obtained by forward modelling, all the information on the system like the waveform of the excitation source, the IR of the antennas, the antenna pattern, the attenuation and dispersion in the ground, *etc.* are included.

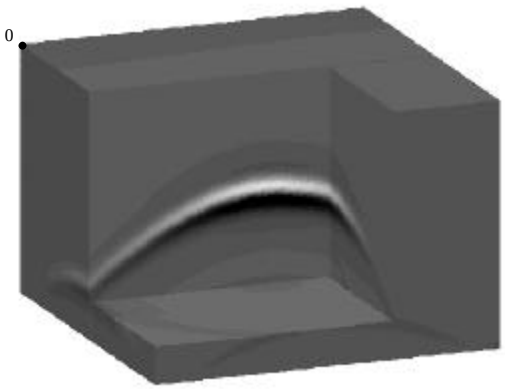

Fig. 4: Synthetic C-scan of a fictive point scatterer at a depth of 6 cm below the air-ground interface, calculated by forward modelling

Although the point spread function $w(x, y, z_o, t)$ is space variant (function of z_o), its shape will not change very much with depth. In practice, the point spread function for a given depth can be used for a broad depth range. As a consequence, the space-time convolution (7) can by considered as space (depth) invariant and the image of the 3D scattering matrix $\hat{\Lambda}(x, y, t)$ can be calculated in one step by

$$\hat{\Lambda}(x, y, t) = b(x, y, t) \otimes_{x,y,t} w(x, y, z_o, t)^{-1} \qquad \textbf{(8)}$$

where $\hat{\Lambda}(x, y, t)$ denotes the spatial image of $\Lambda_{zo}(x, y, t)$, *i.e.* the migrated image,
$b(x, y, t)$ is the recorded C-scan that is to be migrated, and
$w(x, y, z_o, t)$ the point spread function for a fixed depth $z = z_o$.

4. RESULTS OF THE MIGRATION METHOD

The migration by deconvolution is applied on data taken by a laboratory UWB GPR [5], with the antennas mounted on the indoor xy-scanning table. The data are acquired over an area of 50 cm by 50 cm with a step of 1 cm in both x - and y - direction. Fig. 5 shows the results of the migration method on a piece of 20 cm barbed wire, buried at 5 cm of depth in sand. Subplot (d) represents a two-dimensional C-scan of the migrated image. The shape of the barbed wire in Fig. 5 (d) can be easily distinguished and even contains the three sets of pins, present on the real wire. Note that the dimensions of the object in the migrated images approach the dimensions of the real objects.

The aim of migration is to focus reflections on objects back into the true physical shape of the object but also into its true position. To illustrate the latter, we show in Fig. 6 (a) the raw B-scan on an oblique mine. The mine was buried under an angle of about 30° in dry sand, with the highest point of the mine at a depth of 5 cm. In the raw B-scan at the left, the strongest reflections on the mine are found in the lower right corner of the image, whereas in reality the mine is situated in the middle of the image, indicated by the rectangular box in the image. The explanation for this shift is simple. When the antennas are right above the oblique mine, the mine will have a strong reflection in a direction away from the receiving antenna. For the antennas in the direction perpendicular to the flat top of the mine, the reflections on the mine towards the receiving antenna will be stronger than in the case the antennas are right above the oblique mine, leading to a displacement of the target in the raw data. After migration by deconvolution however, the target is found in its true position, as shown in Fig. 6 (b). The migrated image not only shows the object in its true position, but also clearly shows that the object is oblique. Other migration methods, like Kirchhoff migration [2] and f-k migration [2] were also applied on the same data, but with less good results than the migration by deconvolution method. Fig. 6 (c) shows the result after Kirchhoff migration. The migrated image is better than the raw one, but the Kirchhoff migration is not able to bring the target completely back in its actual position.

The previous results are obtained on data that is acquired in the laboratory, where all conditions are well controlled and where the air-ground interface is flat. In reality this is not the case. Ground characteristics like permittivity and attenuation are often not known and have to be estimated. The air-ground interface can be very rough and can introduce additional clutter, which eventually might interfere with the reflections on the target. Furthermore, the ground is not always homogeneous and it can be expected that the UWB GPR, which yields a high resolution, is sensible to these inhomogeneities. The data represented in the Fig. 7 is acquired over an area of 50 cm by 50 cm in steps of 2 cm (which is still small enough to avoid aliasing in the x - and y - direction). Fig. 7 shows a 2D representation of a B-scan and a C-scan of a PMN mine, buried in gravel at a depth of 5 cm, before and after migration. In the images of the raw data there is a lot of clutter present and the shape of the mine is not clear. After migration, most of the clutter disappeared and the circular shape and dimensions of the mine becomes correct.

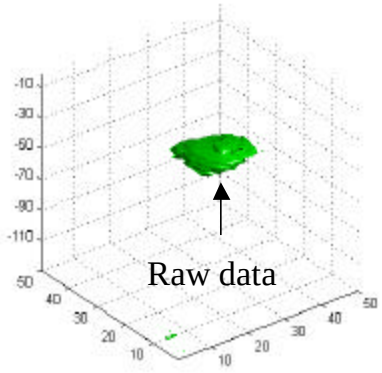

(a) (b)

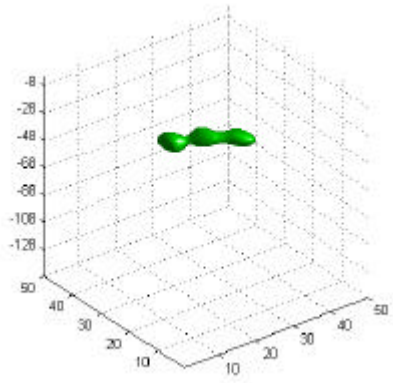

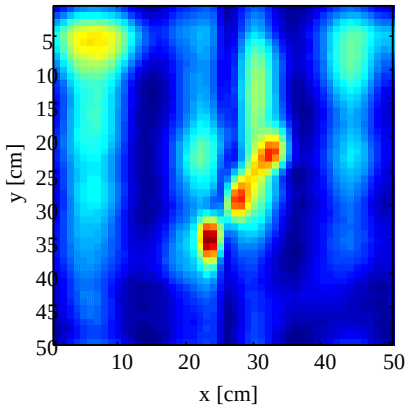

(c) (d)

Fig. 5: Migration by deconvolution applied on barbed wire (length of 20cm) buried at 5 cm

(a) Photo of the barbed wire
(b) 3D C-scan representation of raw data
(c) 3D C-scan representation of migrated data
(d) 2D C-scan representation of migrated data

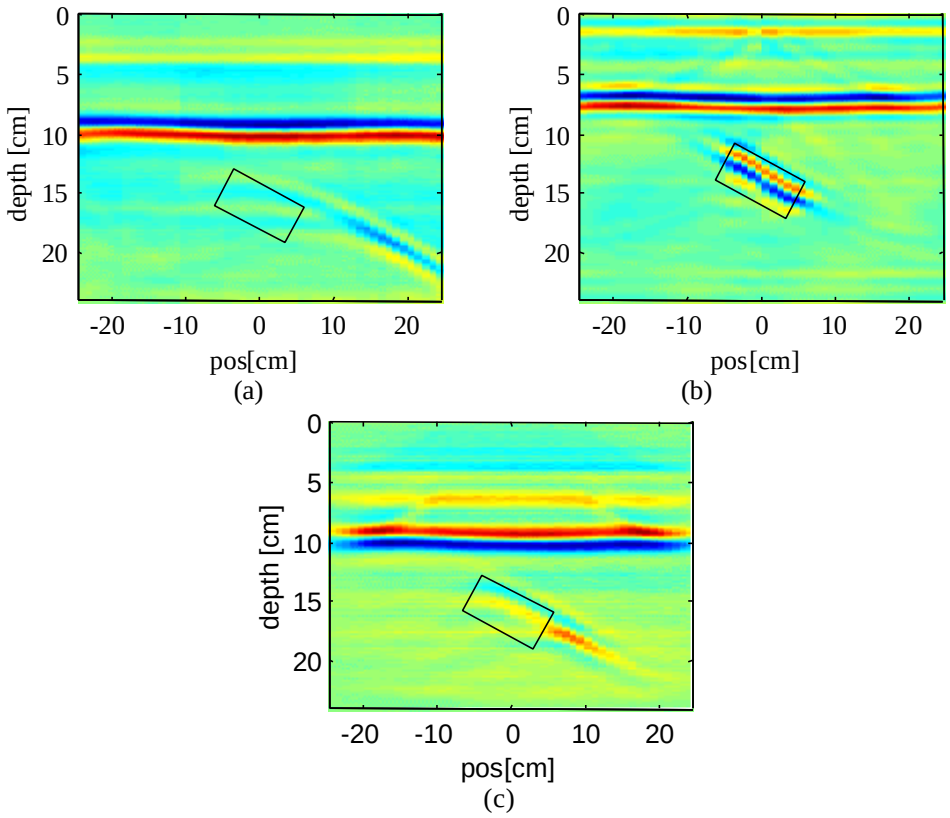

Fig. 6: Oblique PMN mine under an angle of 30°

(a) Raw data
(b) After migration by deconvolution
(c) After Kirchhoff migration

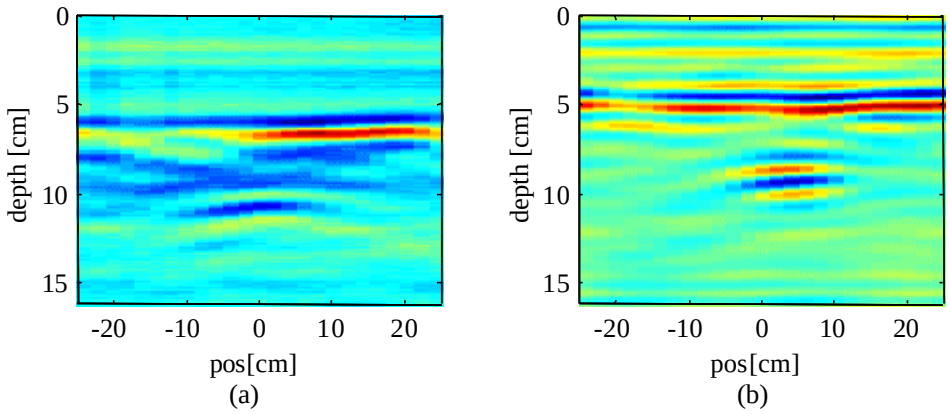

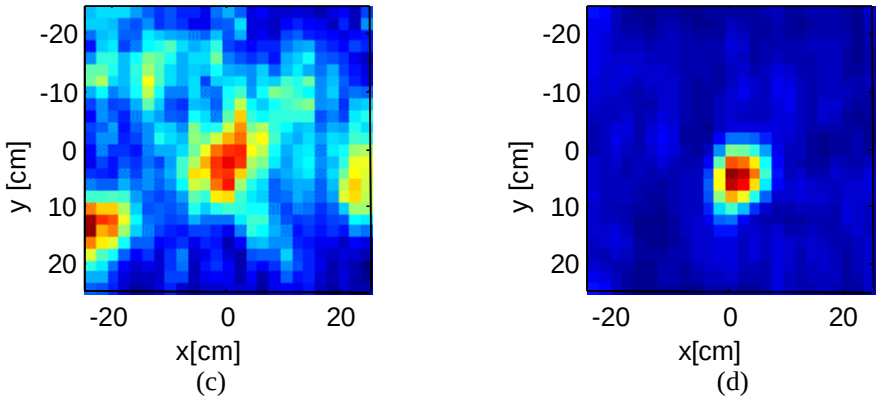

Fig. 7: PMN mine in gravel at 5 cm of depth

(a) B-scan of raw data
(b) B-scan of migrated data
(c) 2D C-scan representation of raw data
(d) 2D C-scan representation of migrated data

5. CONCLUSIONS

The raw C-scans recorded by a GPR are often difficult to interpret for an operator. Due to the beam-width of the antennas, a target in the ground is already seen by the GPR system even when it is not exactly under the antennas. As a consequence, the recorded data will be unfocussed. Focussing techniques to reduce the influence of the beamwidth of the antennas are called migration techniques. Most of the existing migration techniques however do not take into account the characteristics of the acquisition system and the ground characteristics. We therefore proposed a migration technique, called the migration by deconvolution. The novelty of the algorithm is that it uses the time domain model of the GPR and hence does take into account the system and ground characteristics. The migration method is simple and fast. We calculate by forward modelling a synthetic point spread function of the UWB GPR. This point spread function is then used to be deconvolved from the recorded data. The method is evaluated on data coming from the UWB GPR. The results of the migration method are found to be very good and in any case better than conventional migration methods like Kirchhoff or f-k migration. After migration of the data, the UWB GPR give enough resolution in the lateral directions to give an idea of the shape and, in favorable circumstances, of the dimensions of the buried object. The migration method is also able to focus reflection on oblique objects back into their true position and reduces considerable the clutter in a GPR image.

REFERENCES

1. Yilmaz, O., *Seismic data processing*, Society of Exploration Geophysicists, Tusla, OK, 1987.
2. Berkhout, A. J., "Wave field extrapolation techniques in seismic migration, a tutorial", *Geophysics*, **46**, pp. 1638-1656, 1981.
3. Scheers, B., Acheroy, M., Vander Vorst, A., "Time Domain Simulation and Characterisation of TEM Horns Using Normalised Impulse Response", *IEE Proceedings - Microwaves, Antennas and Propagation*, **147**, no. 6, pp.463-468, 2000.
4. Farr, E.G., Baum, C.E., "Time Domain Characterization of Antennas with TEM Feeds", *Sensor and Simulation Notes*, note 426, Air Force Research Laboratory, USA, 1998.
5. Scheers, B., *Ultra-Wideband Ground Penetrating Radar, with application to the detection of Anti Personnel Landmines*, Doctoral thesis, Université catholique de Louvain and Royal Military Academy, Belgium, Mars 2001.